44th AIAA Aerospace Sciences Meeting and Exhibit
9 - 12 January 2006, Reno, Nevada

AIAA Paper 2006-0414

Sonic Boom Computations for Double-Cone Configuration Using CFL3D, FUN3D and Full-Potential Codes

Osama Kandil[1] and Isik A. Ozcer[2]
Aerospace Engineering Department, Old Dominion University, Norfolk, VA 23529

ABSTRACT

Development of highly accurate computational codes for both near-field and far-field sonic boom problem is the focus of this paper The structured-grid CFL3D code is modified using a new, highly accurate grid-adaptation and shock-fitting scheme for supersonic near-field domain prediction. The modified CFL3D code is applied to a double-cone configuration at Mach numbers of 1.26 and 1.41. Because of its sophisticated grid adaptation methodology, the unstructured-grid FUN3D is also used for the near-field computations at Mach number of 1.26. The computed near-field results are compared with the available experimental data. The FUN3D code results and the CFL3D results at an interface located at h/L = 2 (altitude height/body length) are used to generate input data for the highly efficient, far-field, structured-grid full-potential (FP) code. The relative errors for the velocity components, at the interface h/L = 2, between the results of the unstructured-grid FUN3D code and the results of the structured-grid FP far-field code are computed and presented. Next, the FP Far-field code is used to advance the solution from h/L = 2 to h/L = 6, 10 and 18 and the results are compared with those obtained from matching FP with FUN3D, matching FP with the modified CFL3D, and the experimental data. The interface results have also been advanced to a far-field location at h/L = 40. The conclusion of this study is that the FUN3D code is highly accurate for near-field and far-field computations. The grid adaptation and shock fitting scheme has to be used in the FP code and CFL3D code for obtaining highly accurate results.

---

1. Professor and Eminent Scholar, Associate Fellow AIAA
2. PhD Graduate Research Assistant, Member AIAA.

1. INTRODUCTION AND BACKGROUND

In the sonic-boom propagation problem, the use of a high-order methodology in the far- field computations is feasible and desirable. Ideally, this "high-order" solution would be matched to the near-field solution point for point including radial gradients and shock jumps. In Ref. 1 by the author and his co-workers, the near-field flow is predicted by using the Euler equations code CFL3D (as in other approaches) while the mid- and far-field flows are predicted by using a newly developed full-potential (FP) equation methodology. This scheme is called the Euler full-potential (EFP) scheme. Once shocks are captured, a grid adaptation scheme, based on the density gradient, is implemented to obtain a crisper shock. This is followed by a shock-fitting scheme that is based on a search algorithm along with the application of the Rankine-Hugoniot conservation equations of mass, momentum and energy equations. The repetitive solution cycles of the grid-adaptation and shock-fitting (GASF) schemes minimize the relative errors in the mass, momentum and energy across the predicted shocks. An interface-plane matching methodology has been developed to transfer the Euler near-field results to those of the full-potential far-field computations. The sensitivity of the computed ground pressure jump to the location of this interface plane has been studied for both a delta wing and an aircraft configuration, and the results were satisfactory.

Applications of EFP and GASF codes have been made to a 60 degree Delta wing with a 5 percent thickness ratio biconvex airfoil section. The wing has various chords, lift coefficients and flight altitudes. The propagation code has been also applied to complete aircraft configurations at various supersonic speeds and altitudes, such as a modified F-5 aircraft (Ref. 2), the “Baize-Coen” configuration (Ref. 3) and a wing-body configuration reported by Susan Cliff (Ref. 4). Typical ground pressure results of this code for

delta wings have been compared with those computed using the linear ray-tracing code of Plotkin, Ref. 5 (Thomas methodology). Experimental data and real field measurements were used in these comparisons in order to validate the predicted results.

Unstructured grid technology promises easier initial grid generation for novel complex three-dimensional (3D) configurations as compared to the structured grid techniques. The use of unstructured grid technology for CFD simulations allows more freedom in adapting the discretization of the meshes to improve the fidelity of the simulation. Many previous efforts attempted to tailor the discretizations of unstructured meshes to increase solution accuracy while reducing computational cost, Ref. 6.

Most of these adaptive methods focus on modifying discretizations to reduce local equation errors. These local errors are not guaranteed to directly impact error in global output functions. These methods, often referred to as feature-based adaptation, focus on resolving discontinuities or strong gradients in the flow field. Unfortunately, flow features (e.g., shocks) can be in the incorrect location due to errors elsewhere in the flow field. Also, resolving the flow in a location with large local error may have a minimal effect on the output function (e.g., a downstream shock). The Fully Unstructured Navier-Stokes Three-Dimensional FUN3D (Refs. 7 and 8) is a compressible flow solver which employs an unstructured finite-volume tetrahedral method for conserved variables. To speed execution, the global problem domain is decomposed into multiple subdomains and the flow and the adjoint problems are solved with a parallel execution scheme, which communicates via the message passing interface (MPI) standard.

The FUN3D Code accuracy is being evaluated for the near-field computations for capturing shocks and adapting the unstructured grid. The adjoint variable approach (solution of the dual problem) is an efficient method for computing derivatives of a function of interest for gradient-based design methods. Some examples of discrete adjoint design methods are given in Anderson[7] and Nielsen [8]. The combination of adjoint-based grid adaptation and design techniques can yield an attractive tool for the aerodynamic design of new configurations. Adjoint-based error prediction and adaptation can yield meshes with fewer points than traditional feature-based schemes with computable error estimates on output functions. Design processes require analysis and derivative evaluation tools that operate with minimal human interaction. Robust, automatic adaptation techniques enable the increased use of nonlinear flow calculations in larger multidisciplinary design frameworks. These new techniques enable efficient analysis for existing configurations and expanded exploration of design spaces for new configurations. This work was part of the Fast Adaptive Aerospace Tools20 (FAAST) program. The goal of the FAAST program was to improve the robustness of high-fidelity CFD analysis and reduce total time for analysis and design.

In the present paper, the FUN3D code is applied to a double-cone configuration at a Mach number of 1.26. The CFL3D code is modified by using a new SFGA scheme and is applied to the same double-cone configuration with Mach number of 1.26 and 1.41. The results of the two codes are compared with the experimental data of Ref. 9. Next, an interface-plane interpolation scheme has been developed between the FUN3D code and the efficient FP Far-field code at an altitude to configuration length of h/L= 2. The interpolation errors have been computed. The same matching is done with the modified CFL3D. Next, the FP code is modified using the same SFGA scheme, and used to propagate the interface results to h/L = 6, 10, 18 and very high far-field locations as well. The results of the FUN3D-FP coupled code and the modified CFL3D-FP coupled code are compared with the experimental data.

2. DOUBLE-CONE CONFIGURATION

Figure 1 shows a side-view and a three-dimensional view of the double-cone configuration that is used for the present computational applications and the experimental data, Ref. 9. The flow Mach numbers are 1.26 and 1.41 and the angle of attack is zero.

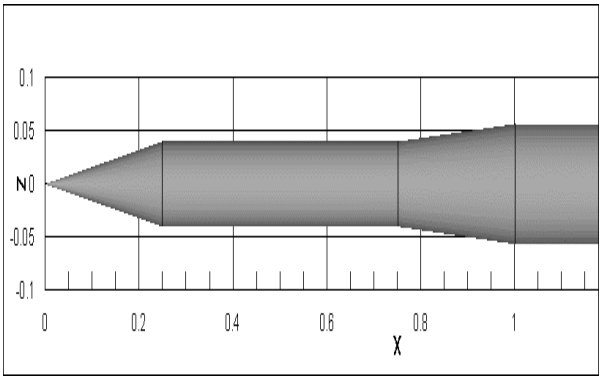

$$r = x\sqrt{\frac{0.08}{\pi}} \qquad (0 \le x \le 0.25)$$

$$r = \frac{1}{2}\sqrt{\frac{0.02}{\pi}} \qquad (0.25 \le x \le 0.75)$$

$$r = \frac{1}{2+\sqrt{2}}\sqrt{\frac{0.04}{\pi}}\left(2x - \frac{2-\sqrt{2}}{2}\right) \qquad (0.75 \le x \le 1.00)$$

$$r = \frac{1}{2+\sqrt{2}}\sqrt{\frac{0.04}{\pi}}\left(2 - \frac{2-\sqrt{2}}{2}\right) \qquad (x \ge 1.00)$$

where x and r are nondimensionalized with the body length

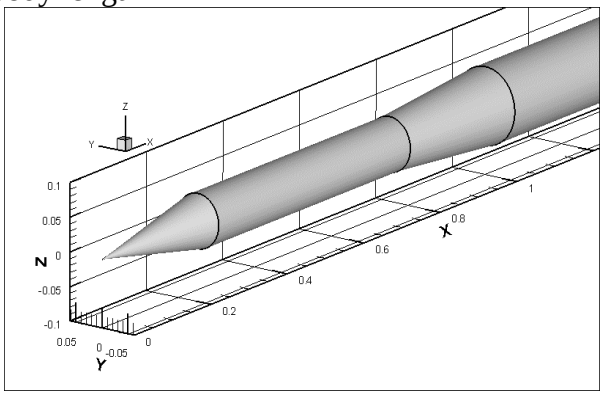

Figure 1: Side-view and three-dimensional view of the dimensionless double-cone configuration (Ref. 9).

3. GRID-ADAPTATION AND SHOCK-FITTING (GASF& SFGA) NEW SCHEMES

Old GASF Scheme:

The original grid-adaptation shock-fitting (GASF) scheme has been updated for use with the CFL3D code for the present application of double-cone configuration. It has been used also in the FP far-field scheme. First the flow is solved on an initial grid using the Euler equation solver of the existing CFL3D. Once the shocks are captured, then the GASF solver is turned on. First, the method adapts the grid around the captured shock(s) according to the density gradient without distorting the grid cell aspect ratio. Next, the captured shock(s) is fitted physically using the Rankine-Hugoniot equations on piecewise segments of the captured shock(s). The focus is to secure conservation of mass, momentum and energy across shock(s). If the fitted piece-wise shock segments produce non-smooth shock surface, then the physical shock-fitting is followed by a geometrical shock fitting. Here, a high-order polynomial is used for the geometrical shock fitting. Geometrical shock fitting is a must for the grid adaptation step of the next GASF iteration cycle. The GASF cycles are repeated until the average errors across a shock(s) in mass, momentum and energy reach a prescribed minimum value.

New SFGA Scheme (Method 1) and SFGA Scheme (Method 2):

Here, physical shock fitting is accomplished using the gradient of density and Mach on the coordinate line crossing the shock. This coordinate line is designed to be ξ^2 associated with the grid index j. The gradients are computed by central differencing. Gradient of density is evaluated in the Cartesian system, $|\nabla\rho|$ whereas gradient of Mach is limited to the derivative of Mach with respect to ξ^2 only, $\partial M/\partial\xi^2$. Both of these gradients peak at the shocks, and stay mostly leveled in the remaining regions. Thus, they form sets of data that can be used to locate shocks in the solution. Theoretically, this data should be a smooth curve with peaks occurring only at shocks. However in practice, the CFD solution is not perfect and sometimes this data contains noise. This complicates the automation of shock detection process, since oscillations in the noise can easily be mistaken for a shock. Fortunately, peaks at shocks are almost always higher than the noise oscillations, and the noise can be filtered out by utilizing a threshold value during the analysis of the data. This threshold value ε_{dM} is specified by the user.

At each shock, a number of points are found to be above the threshold in both data sets. This number decreases as the solution gets better with each shock-fitting iteration, but rarely is one. Hence it is not correct to state that each point above the threshold represent a single shock. Instead at each peak, points above the threshold are grouped together, and

the one with the highest $|\nabla\rho|$ among the others in the same group is chosen to be the shock point. Hence the physical fitting process is completed in two basic steps. The first is to locate these separate groups of points above the threshold, and the second is to find the one with highest $|\nabla\rho|$ in each group.

Since the idea is to eventually obtain each shock on a single grid line, Rankine-Hugoniot (R H) equations are to be used across a single grid line. The J indices of the starting points of the captured shocks ($J_{ns,1}^{SHOCK}$) indicates the gridline that R H equations will be used across. The normal direction that is to be tested is obtained by using the slope of the grid line. At each k, the cell centers one upstream and one downstream of this $J_{ns,1}^{SHOCK}$ are used to check on the differences in mass, momentum and enthalpy. Depending on the magnitude of the error, one can cease to continue with the next iteration. If the errors are large enough, the grid generation process for the captured shock will begin. The captured shock points are fitted with 5^{th} order polynomials to come up with an algebraic equation that can be used in the grid generation process. Polynomials of 3^{rd} order can also be used, however, it has been seen that 5^{th} order polynomials fit the endpoints better than 3^{rd} order, which is important for the grid generation subroutine.

The polynomial coefficients are input to the grid generation subroutine, along with the dimensions and coordinates that define the body, and the grid is generated. The polynomials for the shocks are used to create foundation gridlines for the block. Inflow and outflow boundaries are created by translating that polynomial that is closest to that boundary by some units. Grid adaptation is also based on the density gradients. The grid lines are clustered towards regions of high density gradients, making an efficient use of the available grid points and eliminating the use of excess number of grid points. Additional details of the new SFGA scheme can be found in Ref. 10.

4. RESULTS OF NEW SFGA SCHEME APPLIED TO CFL3D CODE FOR DOUBLE-CONE CONFIGURATION

Figures 2-9 show the sequence of the grid shape and corresponding density contours of the new SFGA scheme (method 1). The application here is for the double cone with M_∞ = 1.26. Notice here that the new SFGA scheme (method 1) is emphasizing shock fitting more than grid adaptation. For instance in

Figs. 8 and 9, SF2-GA1-SF1-GA1-SF5 sequence is used, where SF stands for shock fitting and GA stands for grid adaptation. The new SKGA scheme is obviously producing sharper accurate shocks without overshooting. Table 1 shows 2 results of the average percentage errors in mass, momentum and energy across the shocks after 10 and 11 cycles of SF and GA

A second method (method 2) is developed, where the physical and geometrical shock fitting and grid adaptation are coupled through the use of solution interpolation. In this method, the first step is creating a shock fitted grid from the available solution, second step is interpolating the solution to this new grid, and final step is adapting the grid lines for the high density gradient regions. Shock fitting has to be done before grid adaptation, in order to maintain the shock fitted grid lines. Grid adaptation code recognizes the shock fitted grid lines in this grid by using the same shock search and detection algorithms used in shock fitting code, and adapts the regions in between shock lines, without altering the shock lines. This coupled method is named SFGA. It is seen that this second method is much more efficient and accurate than performing separate iterations for SF and GA. Table 2 shows the results of average errors in mass, momentum and energy across the shocks after 5, 6 and 7 cycles of coupled SF and GA. It is observed that the errors are 25% less than those of method 1, and are obtained in less number of SF and GA cycles.

Table 1: Percentage errors in mass, momentum and energy using SFGA method 1.

Grid	% error in mass	% error in mom.	% error in energy
SF2-GA1-SF1-GA1-SF5	0.08780	0.06518	0.01556
SF2-GA1-SF1-GA1-SF6	0.08771	0.06485	0.01516

Table 2: Percentage errors in mass, momentum and energy using SFGA method 2.

Grid	% error in mass	% error in mom.	% error in energy
SFGA5	0.06471	0.05052	0.01362
SFGA6	0.06223	0.04844	0.01300
SFGA7	0.06253	0.04884	0.01324

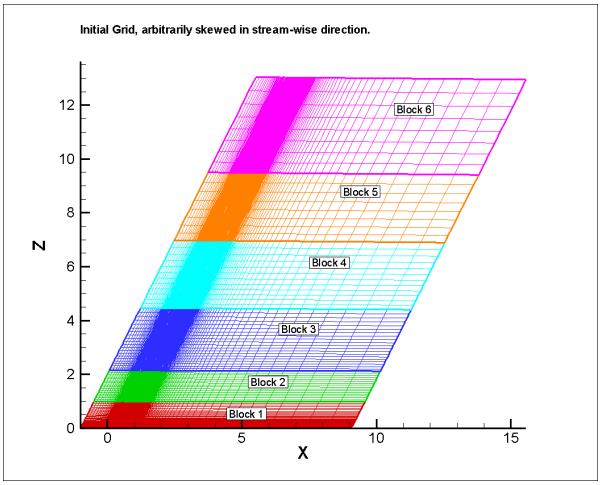

Figure 2: Initial grid with 6 grid blocks.

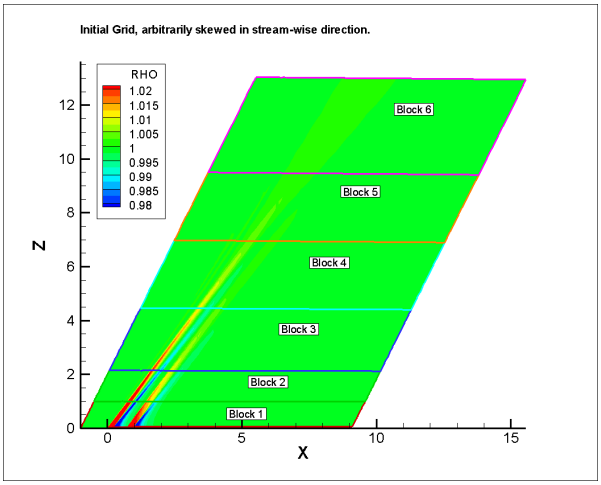

Figure 3: Solution on Initial Grid. Notice that the shocks are dissipated very early.

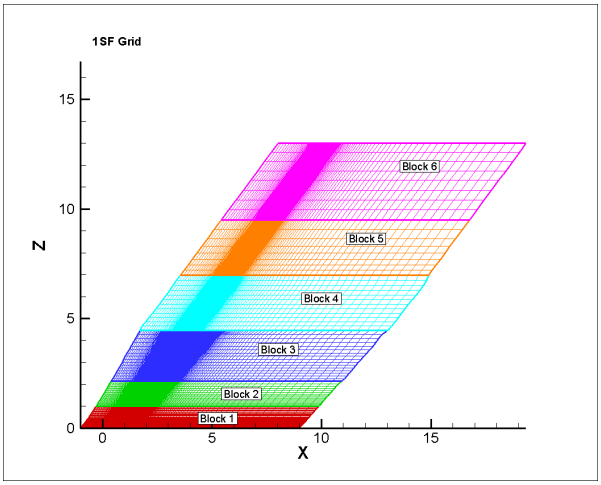

Figure 4: Grid after 1 Shock Fitting. Because the shocks were dissipated in the initial solution, they are not completely detected by the shock search algorithms after block 3.

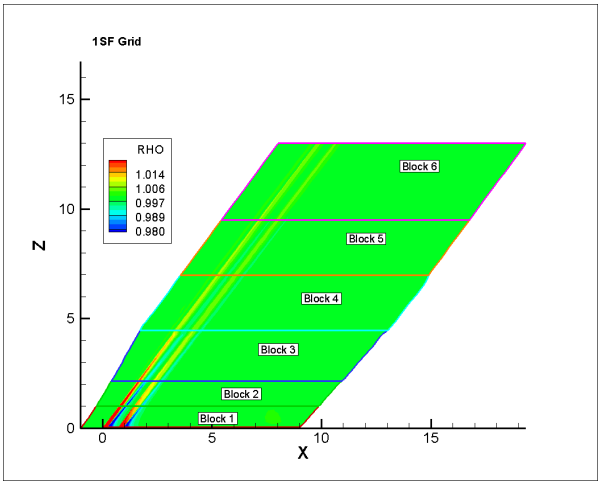

Figure 5: Density contours on the 1 SF grid. By the first fitting iteration, two shocks are captured all the way to the upper limit of the domain.

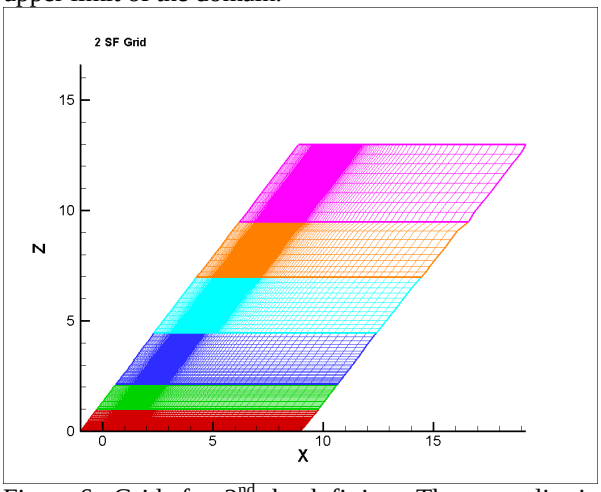

Figure 6: Grid after 2nd shock fitting. The anomalies in the grid have been mostly cured. The grid looks straight and continuous with no bumps or sharp changes.

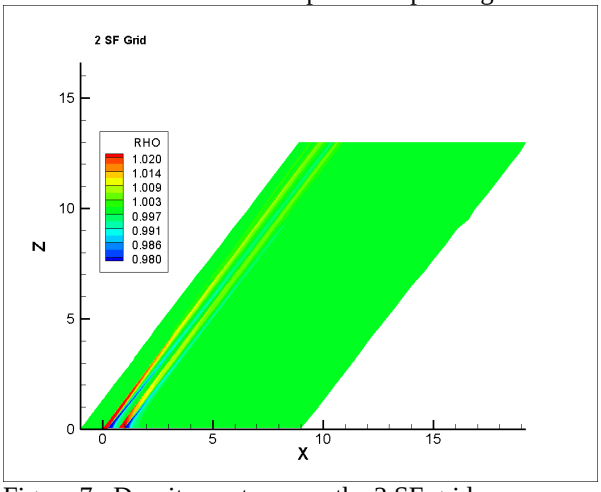

Figure 7: Density contours on the 2 SF grid.

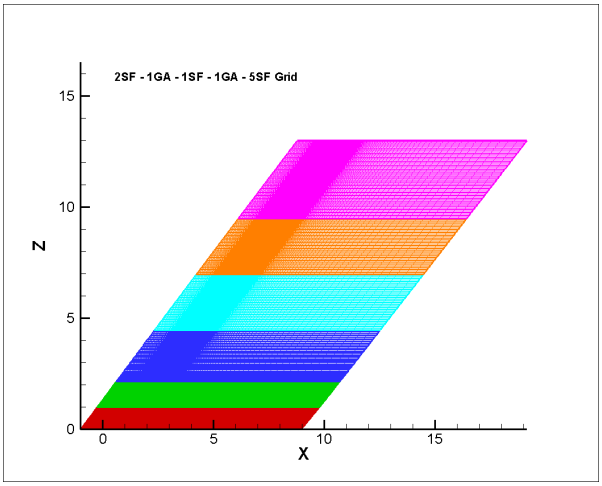

Figure 8: Converged grid after SF2-GA1-SF1-GA1-SF5.

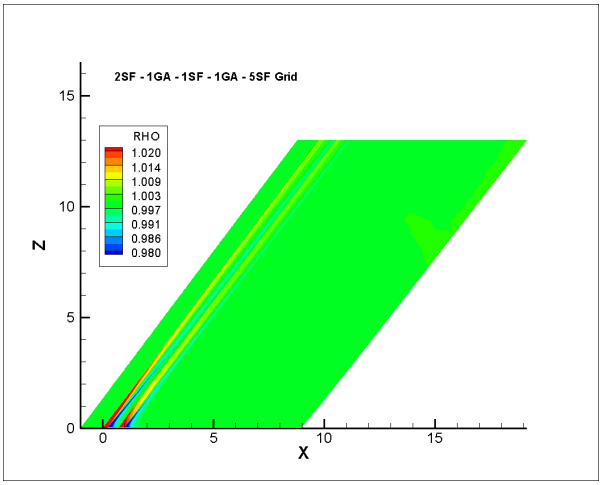

Figure 9: Converged density contours after SF2-GA1-SF1-GA1-SF5.

5. NEAR-FIELD RESULTS AT h/L = 2, 6 AND 10 USING CFL3D WITH NEW SFGA SCHEME

Figures 10-12 show the history curves of the adjusted pressure versus the adjusted x for the modified CFL3D results with the new SFGA scheme (method 2). The curves show the SFGA iterations from SFGA1 to SFGA 7, where the converged shocks are obtained. The history curves are shown for h/L = 2, 6 and 10. It is obviously clear that the new SFGA scheme (method 2) produces a converged solution with sharp and accurate shocks.

Figure 13 show comparisons of the converged solution at h/L = 10 with those of the FUN3D code, the near-field theory and the experimental data of Ref. 9. The modified CFL3D results and the FUN3D results are in good agreement with the experimental data.

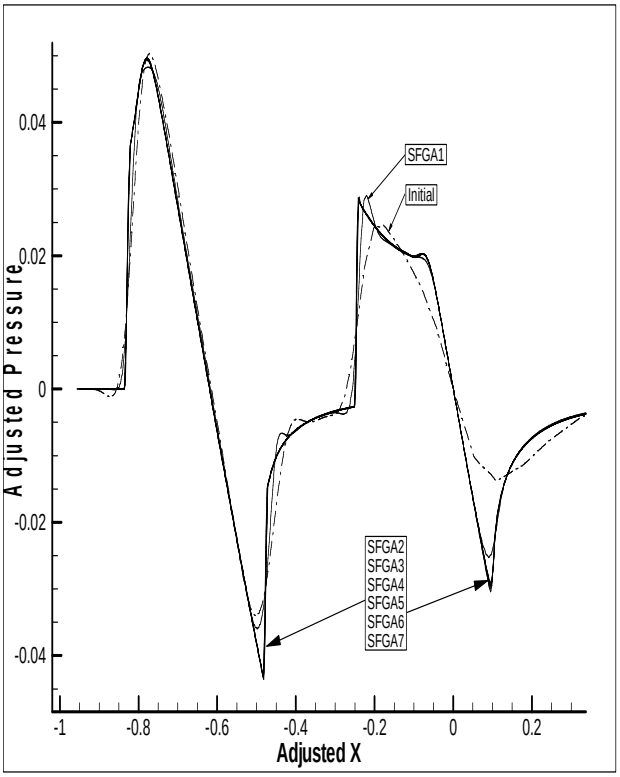

Figure 10: Adjusted pressure signatures at *h/L = 2* obtained at different SFGA steps.

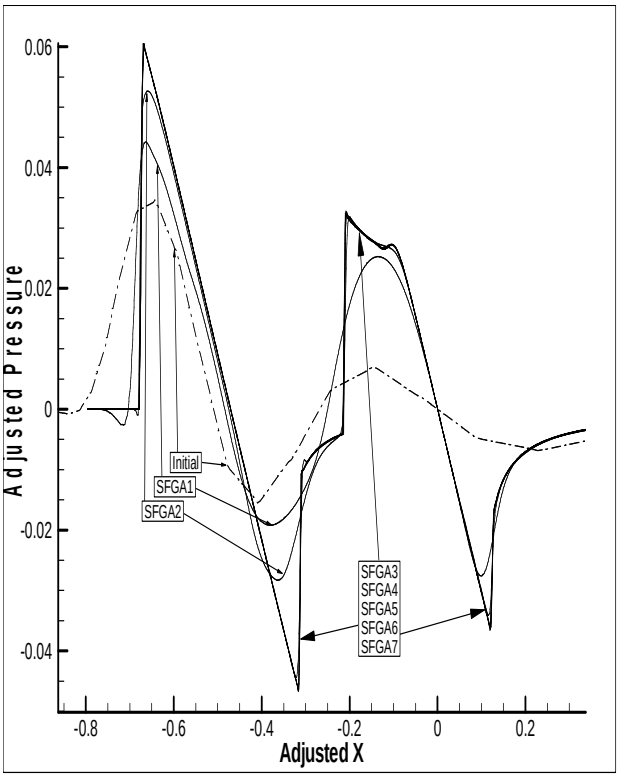

Figure 11: Adjusted pressure signatures at *h/L = 6* obtained at different SFGA steps.

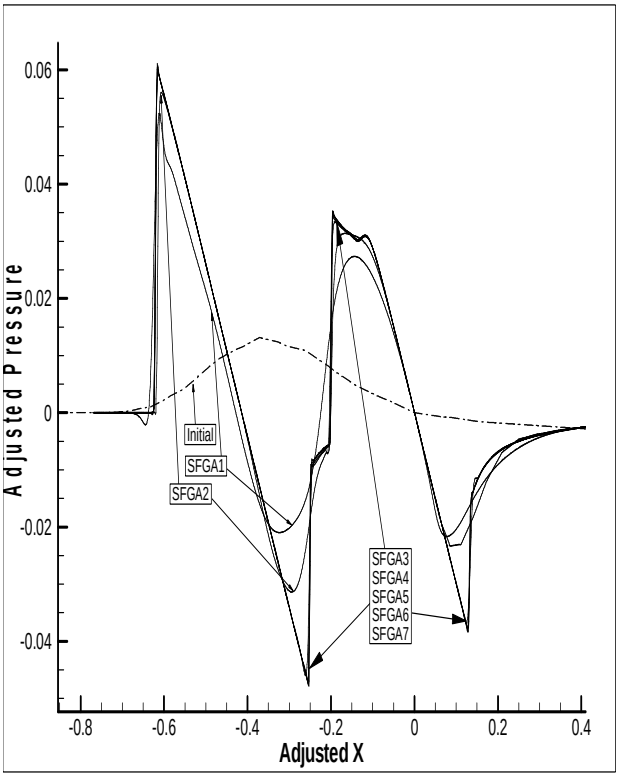

Figure 12: Adjusted pressure signatures at *h/L =10* obtained at different SFGA steps.

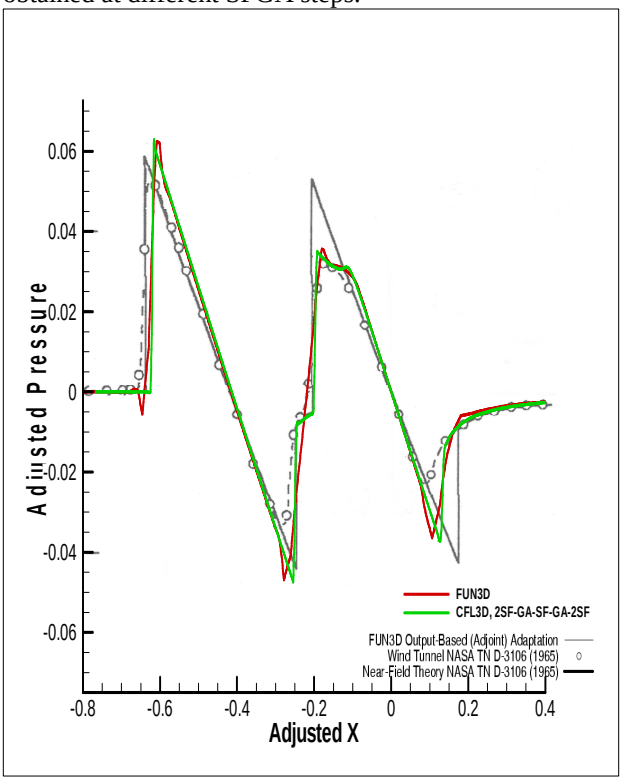

Figure 13: Comparison of the present results and the FUN3D results at h/L = 10 with experimental data.

6. FUN3D INTERFACE MATCHING WITH FP CODE AT h/L =2 & MARCHING TO h/L = 6 -70

Interface Matching between FUN3D and Full-Potential at h/L = 2:

The interface vertical cut is taken from the FUN3D solution at h/L = 2, which is the interface plane location. The FUN3D code results are then fed to the interface code where the Euler variables are converted to velocity potential ϕ. Table 3 shows the average error in U, V, and W between the FUN3D results and the Full-potential results. The error contours in U, V and W at h/L = 2 are shown in Fig. 14. It is obvious that the matching is of high accuracy

Table 3: Average error in the velocity components at the interface

Variable	Average error
U	2.17313e-5
V	1.33605e-5
W	1.35324e-5

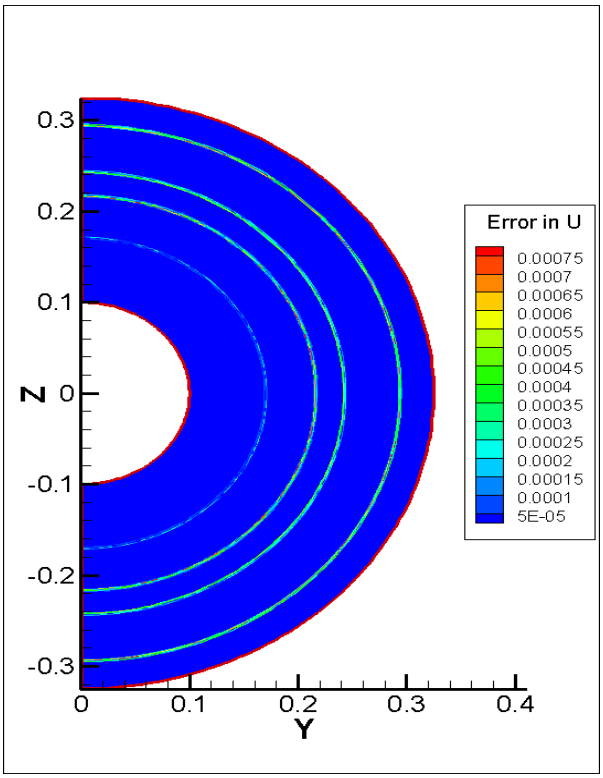

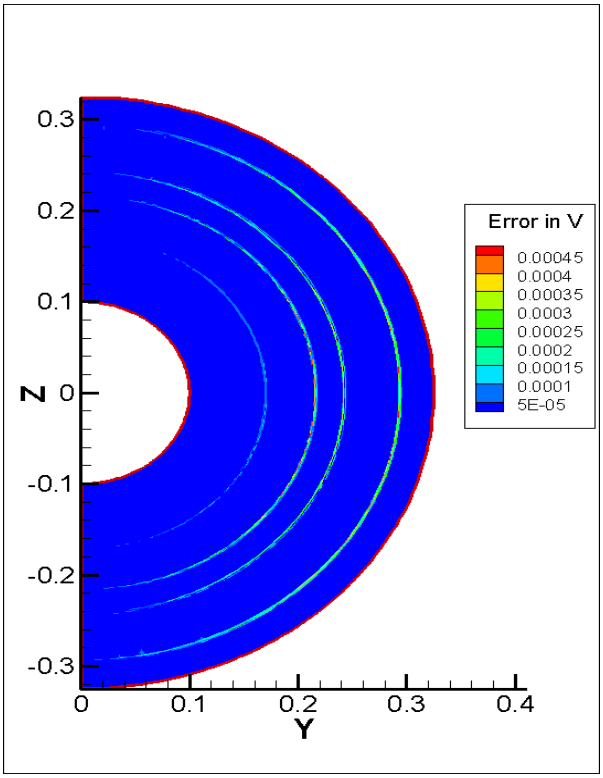

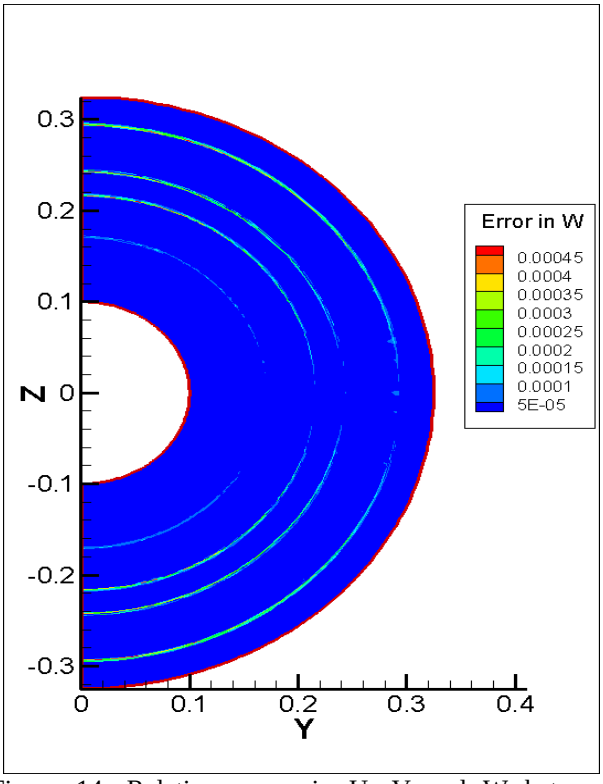

Figure 14: Relative errors in U, V and W between FUN3D and Full Potential at h/L =2.

Full-Potential Marching from h/L= 2 (FUN3D or CFL3D) to h/L = 6 -70 & Comparisons:

The FP matched interface solutions obtained from FUN3D and CFL3d are marched to h/L = 6 and then to h/L =10, 18, 40 and 70. It should be emphasized here that the SFGA scheme is used also with the FP code. Figure 15 shows a comparison of the adjusted pressure versus the adjusted x distance at h/L = 6 of the FP matched with FUN3D and the FP matched with CFL3D. The comparison shows excellent agreement. These results are compared with the experimental data in Fig.16, which again shows excellent agreement. Figures 17 and 18 show similar comparisons as the previous case but at h/L = 10. Figure 19 shows the comparison at h/L = 18 along with CFL3D marching (Euler Solution) to h/L = 18. It is conclusively clear that the FP matching with FUN3D is highly accurate and efficient.

Figures 20 and 21 show comparisons of the adjusted pressure versus the adjusted x distance at h/L = 40 and 70, respectively, of the FP matched with FUN3D and the FP matched with CFL3D.

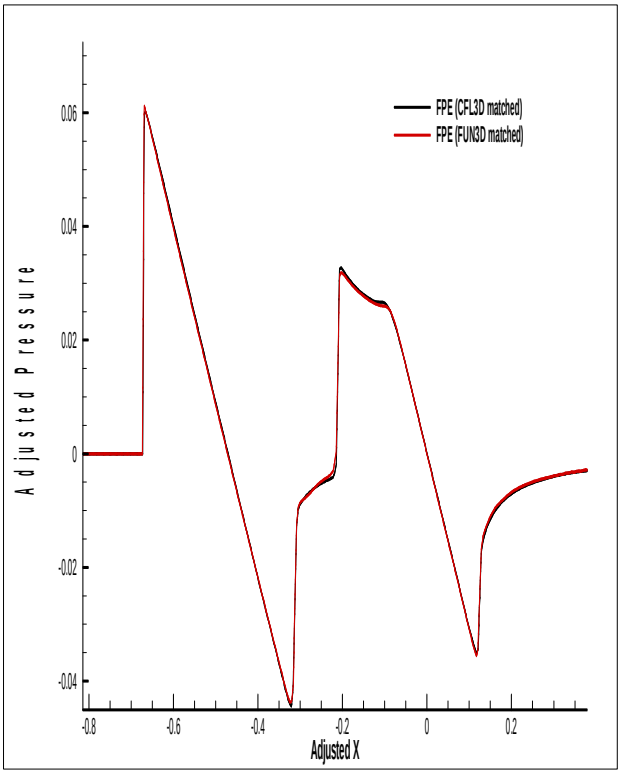

Figure 15: Adjusted pressure signatures at *h/L =6*, comparing both FP matched solutions with FUN3D and CFL3D.

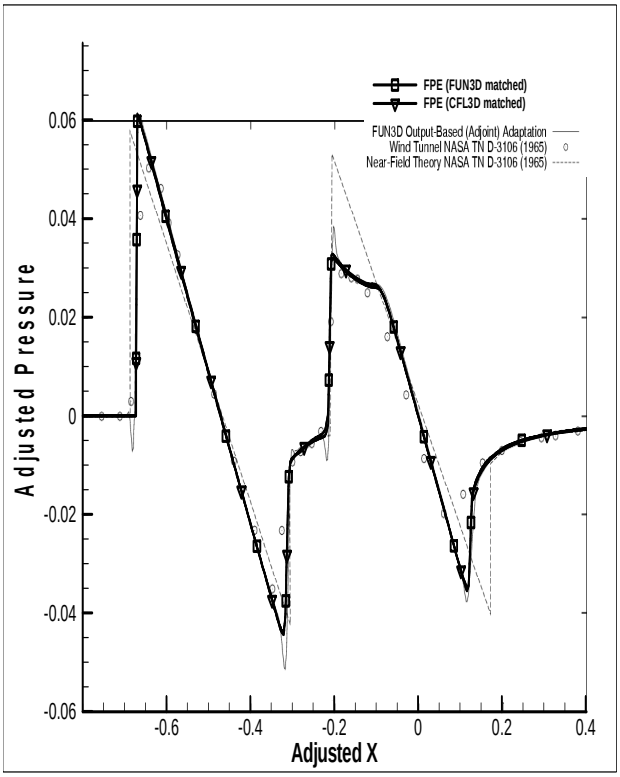

Figure 16: Adjusted pressure signatures at *h/L =6*, comparing both FP matched solutions with FUN3D and CFL3D with the experimental data.

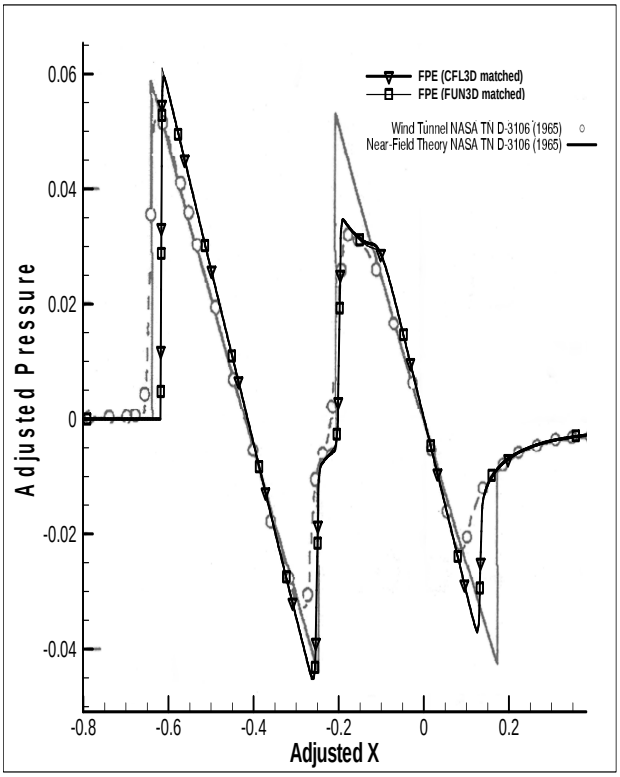

Figure 18: Adjusted pressure signatures at *h/L =10*, comparing both FP matched solutions with FUN3D and CFL3D with the experimental data.

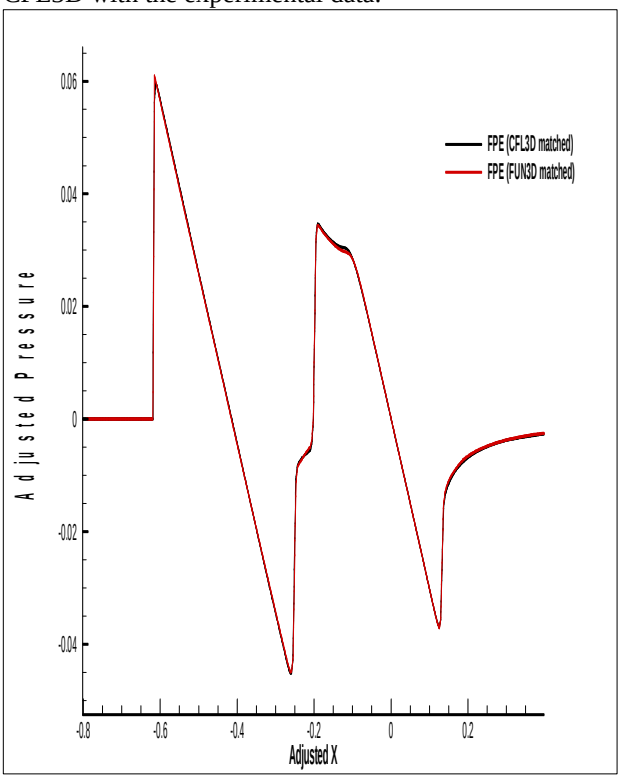

Figure 17: Adjusted pressure signatures at *h/L = 10*, comparing both FP matched solutions with FUN3D and CFL3D.

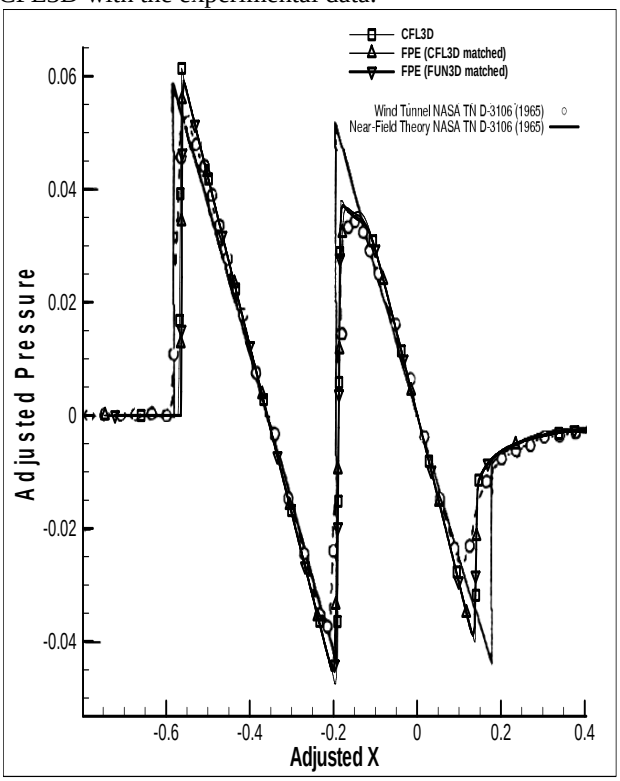

Figure 19: Adjusted pressure signatures at *h/L =18*, comparing both FP matched solutions with FUN3D and CFL3D with the experimental data and CFL3D marching.

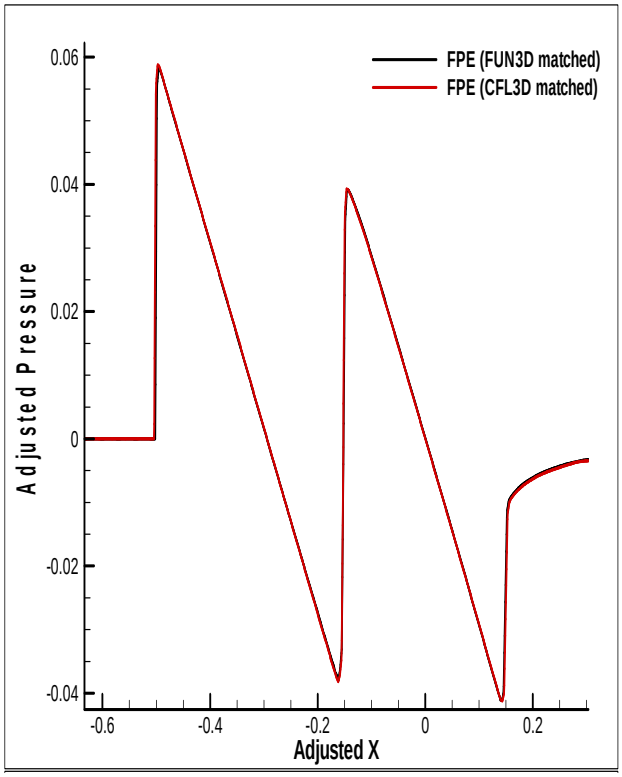

Figure 20: Adjusted pressure signatures at *h/L =40*, comparing both FP matched solutions with FUN3D and CFL3D.

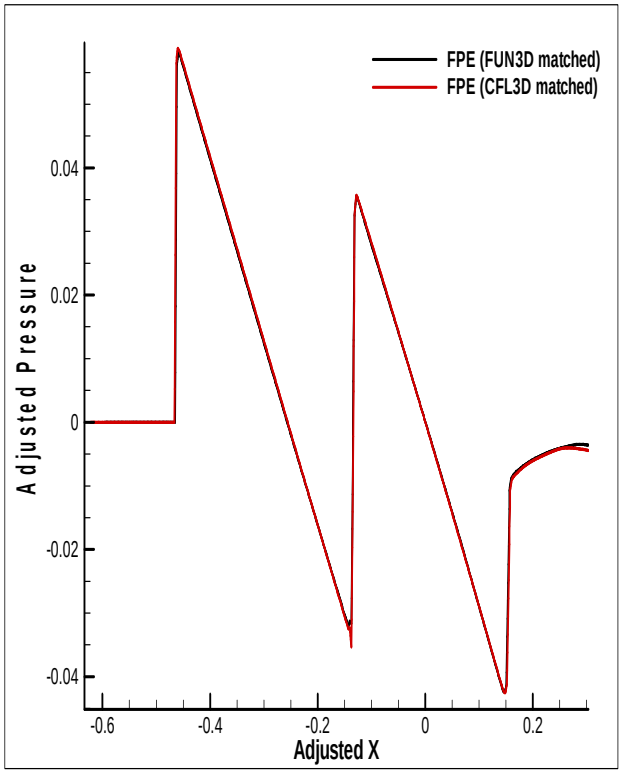

Figure 21: Adjusted pressure signatures at *h/L =70*, comparing both FP matched solutions with FUN3D and CFL3D.

7. DOUBLE-CONE RESULTS FOR M_∞ = 1.41 USING MODIFIED CFL3D AND MATCHING WITH FP CODE

Here we show additional results of the modified CFL3D as applied to the double-cone configuration at M_∞ = 1.41. Figures 22 and 23 show the results of the adjusted pressure versus the adjusted axial distance at h/L = 2 and 10 for 7 SFGA cycles, which couples shock fitting and grid adaptation. It is obviously clear that the scheme produces sharp shocks. Figures 24 and 25 show comparisons with the experimental data at h/L = 5 and 10. Again, the net conclusion is that the SFGA scheme greatly modifies CFL3D code and FP code in producing sharp and accurate shocks.

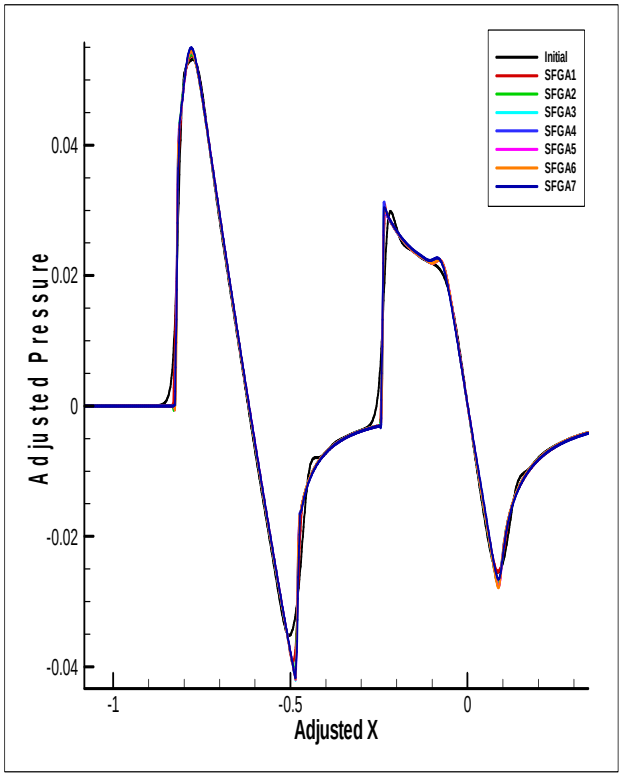

Figure 22: Adjusted pressure signatures at *h/L = 2*, obtained at different SFGA steps, M_∞ = 1.41.

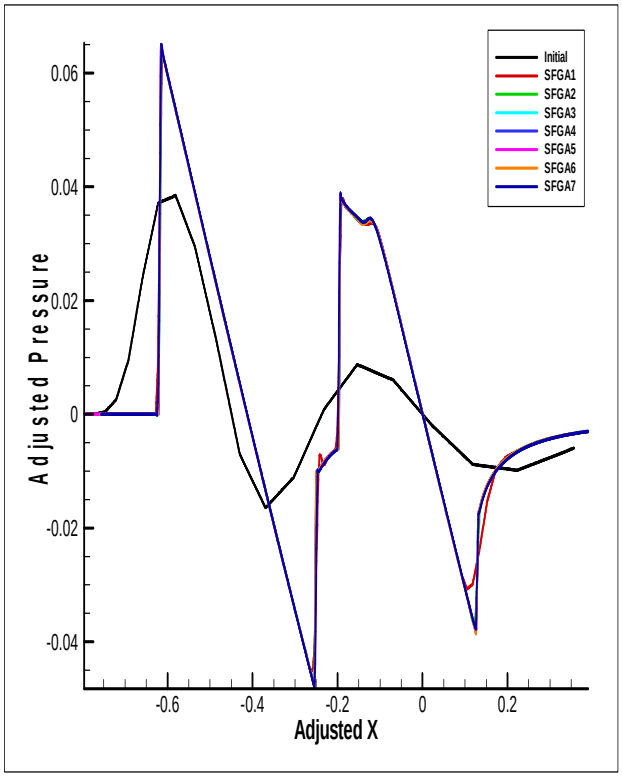

Figure 23: Adjusted pressure signatures at *h/L = 10*, obtained at different SFGA steps, $M_\infty = 1.41$.

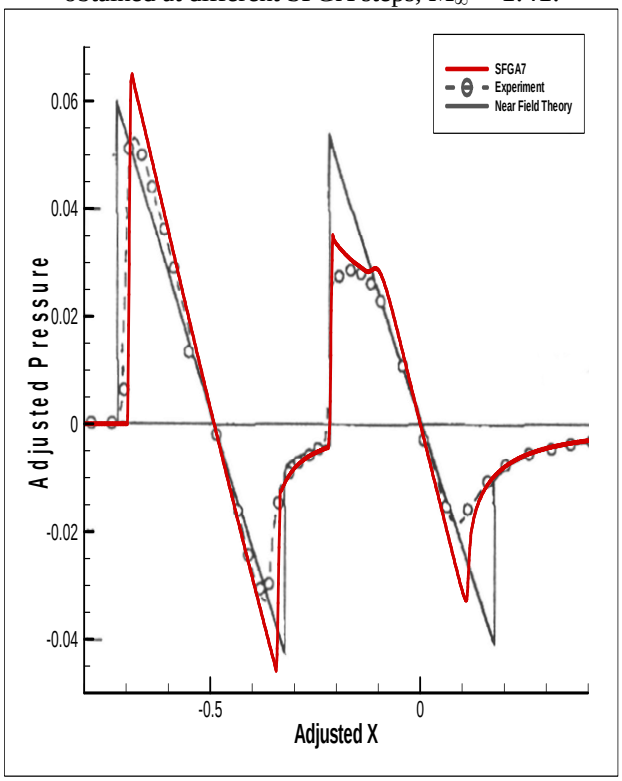

Figure 24: Adjusted pressure signatures at *h/L =5*, comparing FP matched solution with CFL3D with the experimental data.

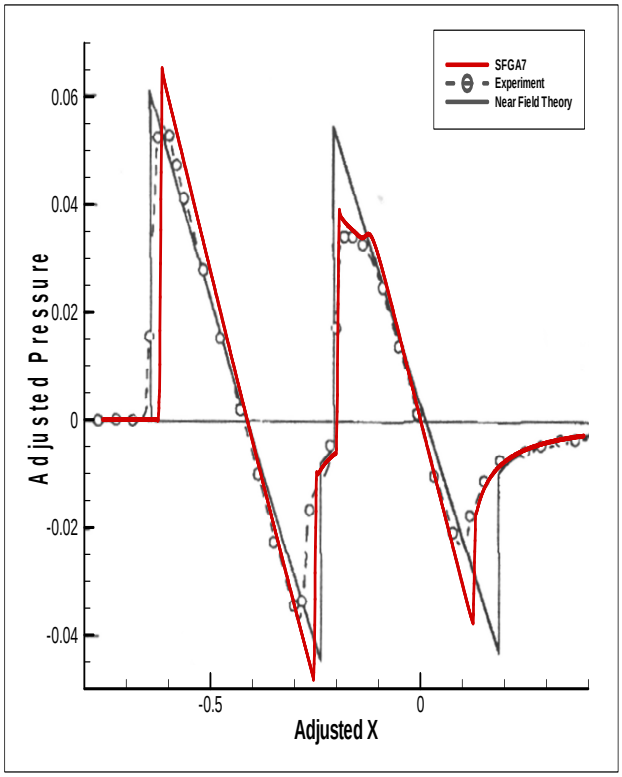

Figure 25: Adjusted pressure signatures at *h/L =10*, comparing FP matched solution with CFL3D with the experimental data.

8. CONCLUSIONS

Research work in this paper has been focused on the development of highly accurate computational codes for both near-field and far-field sonic boom problem. The structured-grid CFL3D code is modified using a new, highly accurate grid-adaptation and shock-fitting scheme for supersonic near-field domain prediction. Two methods have been developed for this purpose, and the second method, which couples shock fitting and grid adaptation, has been shown to be very efficient and more accurate in comparison with the first method, where grid adaptation and shock fitting are carried out separately. The modified CFL3D code is applied to a double-cone configuration at Mach numbers of 1.26 and 1.41. Because of its sophisticated grid adaptation methodology, the unstructured-grid FUN3D is also used for the near-field computations of the double-cone configuration at Mach number of 1.26. The computed near-field results are compared with the available experimental data. The results of the FUN3D and the modified CFL3D are in good agreement with the experimental data. Next, the

FUN3D code results at an interface located at h/L = 2 (altitude height/body length) are used to generate input data for the highly efficient, far-field, structured-grid full-potential (FP) code. The SFGA scheme of method 2 has also been used in the FP code. The relative errors for the velocity components, at the interface h/L = 2, between the results of the unstructured-grid FUN3D code and the results of the structured-grid FP far-field code are computed and presented. They are very small. The same matching step has been applied using the modified CFL3D. Next, the FP far-field code is used to advance the solution from h/L = 2 to h/L = 6, 10, 18. The results obtained from matching FP with FUN3D, matching FP with the modified CFL3D, and the experimental data are compared and show good agreement. The interface results have also been advanced to a very far-field location at h/L = 40. The conclusion of this study is that the FUN3D code is highly accurate and efficient for near-field and FP far-field computations. The use of SFGA scheme is a must in the FP code and CFL3D code for highly accurate results.

9. ACKNOWLEDGEMENTS

This work has been developed under a grant support from the NASA Langley Research Center; Dr. Mujeeb Malik is the technical monitor. The authors would like to thank Dr. Malik for his technical input during the development of this work.

8. REFERENCES

1. Kandil, O. A.; Yang, Z.; Bobbitt, P. J., "Prediction of Sonic Boom Signature using Euler /Full Potential CFD with Grid Adaptation and Shock Fitting," AIAA CP 2002-2543, June 2002.

2. Kandil, O. A., Ozcer, I. A., Zheng, X. and Bobbitt, P. J., "Comparison of Full-Potential Propagation-Code Computations with the F-5E "Shaped Sonic Boom Experiment" Program," AIAA 2005-0013, Reno, NV, January 2005.

3. Baize, Daniel G. and Coen, Peter G., "A Mach 2.0/1/6 Low Sonic Boom High-Speed Civil Transport Concept," High-Speed Research: Sonic Boom, Vol. II, NASA Conf. Pub.10133, Ames Research Center, May 12-14, 1993.

4. Cliff, Susan E., "On the Design and Analysis of Low Sonic Boom Configurations," NASA Conf. Pub. 10133, Ames Research Center, May 12-14, 1993.

5. Thomas, Charles L., "Extrapolation of Sonic Boom Pressure Signatures by the Waveform Parameter Method," NASA TN D-6832, June 1972.

6. Park, M. A., "Three-Dimensional Turbulent RANS Adjoint-Based Error Correction," AIAA 2003-3847, AIAA 16th Computational Fluid Dynamics Conference, Orlando, FL, June 2003.

7. Anderson, W. K. and Bonhaus, D. L., "An Implicit Upwind Algorithm for Computing Turbulent Flows on Unstructured Grids," Computers and Fluids, Vol. 23, No. 1, 1994, pp. 1–22.

8. Nielsen, E. J., Aerodynamic Design Sensitivities on an Unstructured Mesh Using the Navier-Stokes Equations and a Discrete Adjoint Formulation, Ph.D. thesis, Virginia Polytechnic Institute and State University, 1998.

9. Carlson, H. W., Mack, R. J. and Morris, O. A., "A wind-Tunnel Investigation of the effect of Body shape on Sonic-Boom Pressure Distribution," NASA TN D-3106, November 1965.

10. Ozcer, I. A., Sonic Boom Prediction using Euler/Full Potential Methodology, Master Thesis, Aerospace Engineering Department, Old Dominion University, Norfolk, VA, December 2005.